Original Article

JCBFM

Journal of Cerebral Blood Flow & Metabolism
2017, Vol. 37(5) 1803–1819

DOI: 10.1177/0271678X16652631
journals.sagepub.com/home/jcbfm
SAGE

Epileptiform activity and spreading depolarization in the blood–brain barrier-disrupted peri-infarct hippocampus are associated with impaired GABAergic inhibition and synaptic plasticity

Kristina Lippmann[1,2], Lyn Kamintsky[3], Soo Young Kim[4], Svetlana Lublinsky[3], Ofer Prager[3], Julia Friederike Nichtweiss[1], Seda Salar[1], Daniela Kaufer[4], Uwe Heinemann[5,6,*] and Alon Friedman[3,7,*]

Abstract

Peri-infarct opening of the blood–brain barrier may be associated with spreading depolarizations, seizures, and epileptogenesis as well as cognitive dysfunction. We aimed to investigate the mechanisms underlying neural network pathophysiology in the blood–brain barrier-dysfunctional hippocampus. Photothrombotic stroke within the rat neocortex was associated with increased intracranial pressure, vasogenic edema, and peri-ischemic blood–brain barrier dysfunction that included the ipsilateral hippocampus. Intrahippocampal recordings revealed electrographic seizures within the first week in two-thirds of animals, accompanied by a reduction in gamma and increase in theta frequency bands. Synaptic interactions were studied in parasagittal hippocampal slices at 24 h and seven days post-stroke. Field potential recordings in CA1 and CA3 uncovered multiple population spikes, epileptiform episodes, and spreading depolarizations at 24 h. Input–output analysis revealed that fEPSP-spike coupling was significantly enhanced at seven days. In addition, CA1 feedback and feedforward inhibition were diminished. Slices generating epileptiform activity at seven days revealed impaired bidirectional long-term plasticity following high and low-frequency stimulation protocols. Microarray and PCR data confirmed changes in expression of astrocyte-related genes and suggested downregulation in expression of $GABA_A$-receptor subunits. We conclude that blood-brain barrier dysfunction in the peri-infarct hippocampus is associated with early disinhibition, hyperexcitability, and abnormal synaptic plasticity.

Keywords

Blood–brain barrier, hippocampus, inhibition, seizures, synaptic plasticity

Received 14 December 2015; Revised 18 April 2016; 26 April 2016; Accepted 26 April 2016

[1]Institute of Neurophysiology, Charité – University Medicine Berlin, Berlin, Germany
[2]Carl-Ludwig-Institute for Physiology, Leipzig University, Leipzig, Germany
[3]Departments of Physiology and Cell Biology, Cognitive and Brain Sciences, The Zlotowski Center for Neuroscience, Ben-Gurion University of the Negev, Beer-Sheva, Israel
[4]Helen Wills Neuroscience Institute and the Department of Integrative Biology, University of California, Berkeley, CA, USA
[5]Neuroscience Research Center, Berlin, Germany
[6]Excellence Cluster NeuroCure, Berlin, Germany
[7]Department of Medical Neuroscience, Faculty of Medicine, Dalhousie University, Halifax, Canada

*These authors contributed equally to this work.

Corresponding author:
Alon Friedman, Department of Medical Neuroscience, Faculty of Medicine, Dalhousie University, Dennis Chair in Epilepsy Research, Halifax B3H 4R2, Canada.
Email: alon.friedman@dal.ca

Introduction

Acquired epilepsies in the elderly often result from a brain lesion due to trauma, stroke, subarachnoid hemorrhage, tumors, or brain infections.[1] Prospective studies show that following stroke 2 to 11% of patients develop epilepsy, which is often associated with cognitive decline, poor neurological outcome, and increased mortality.[2,3] Spreading depolarizations (SDs) and/or seizures arise spontaneously within and around the ischemic core and seem to be involved in lesion progression and reorganization of the surviving neural network.[4,5] Baseline potassium at first rises mildly in the ischemic zone due to activation of neuronal potassium channels and decline in sodium pump activity,[6–9] reducing the threshold for seizures and SDs.[7] Extracellular glutamate and potassium further increase due to seizures, the initial anoxic, and later spontaneous SDs.[10–13] Anoxic SDs contribute to the generation of the core cortical lesion,[14,15] whereas dying cells in the core may be another source of glutamate and potassium.[16] Glutamate and potassium may in turn facilitate the generation of SDs and seizures in the surrounding cortex. In addition, blood-brain barrier (BBB) opening and astrocytic activation may precede the appearance of post-injury seizures and contribute to epileptogenesis.[17] Within the peri-ischemic brain, the rapid activation of astrocytes further contributes to dysregulation of extracellular homeostasis of water, potassium, glutamate, and GABA. Neuronal expression also changes and includes downregulation of GABAergic receptors,[18] which are crucial for maintaining excitation–inhibition balance within a neural network.

Discrimination between diffusional disturbance of the microenvironment resulting from the ischemic lesion and disturbance of regulatory processes due to BBB dysfunction is difficult. Recently it was reported that intravascular coagulation due to photothrombosis (PT) leads to BBB opening and SDs remote from the primary cortical lesion, often involving the hippocampus.[19,20] The mechanisms underlying SD generation in remote cortical regions are not known. Since the hippocampus has a vascular supply independent of the adjacent neocortex (through the longitudinal hippocampal artery)[21] – it is unlikely that the local interference in neocortical blood supply is the underlying mechanism. Similarly, diffusion of potassium and glutamate from the cortical ischemic core or direct propagation of SDs from cortex to hippocampus is also unlikely but difficult to exclude. However, we hypothesized that the observed BBB opening, associated activation of astrocytes, and downregulation of genes involved in synaptic inhibition account for increased hippocampal susceptibility to seizures and SDs after stroke. We thus used imaging, hippocampal field potential recordings, and gene expression analysis to study the effects of BBB opening on hippocampal physiology and network properties.

Materials and methods

Experimental approaches and ethical approval

All experimental procedures were approved by the Landesamt für Gesundheit und Soziales Berlin (T0228/04, G0114/09). Experiments were conducted according to the European Union Directive 2010/63, the guidelines and provisions for implementation of the Animal Welfare Act at Charité – University Medicine Berlin and the Committee for Ethical Care and Use of Animals in Research of Ben-Gurion University of the Negev. Experiments were reported according to the ARRIVE guidelines (Animal Research: Reporting in Vivo Experiments). We used 119 male Wistar rats (200–300 g, 8–11 weeks old, free nutritional access, FEM Charité, Berlin, Germany and Harlan, Jerusalem, Israel). Photothrombotic stroke was induced in randomly chosen naïve animals using the Rose Bengal method,[19,22] as described.[20] In short, anesthesia was induced with intraperitoneal injection of ketamine–xylazin (1.6 and 0.6 mg/kg body weight (b.w.), respectively). For induction of photothrombosis, the calvarium was exposed to a light beam that was vertically centered 1 mm posterior and 1 mm lateral from bregma using a stereotactic frame. Rose Bengal was administered intravenously (i.v. 20 mg/kg b.w.). The halogen light beam (diameter 3.5 mm) was directed for 15 min onto the intact skull. Following the procedure, the wound was sutured. Postsurgical pain prevention was accomplished by xylocain gel (2%) treatment around the wound and subcutaneous buprenorphin (0.05 mg/kg b.w.) injection. Animals were kept in single cages after surgery; 7 out of 93 animals died during or after operation (sham/stroke).

Magnetic resonance imaging

Magnetic resonance imaging (MRI) was performed under isoflurane anesthesia using a pre-clinical system (Aspect Imaging, M2 high performance MRI, Shoham, Israel). T2-weighted (T2w) images were obtained using fast spin echo sequences (TR/TE/NEX = 3400/74/4). For T1-weighted (T1w) images, gadoterate meglumine contrast agent (Dotarem, Guerbet LLC, Bloomington, IN, USA; 1 ml/kg b.w. plus 0.05 ml for cannula) was injected into the tail vein for up to 24 h and intramuscularly for seven days post-stroke scans. T1w spin echo scans were acquired before (one scan) and after the injection (eight scans) with TR/TE/NEX = 400/14/2. Diffusion weighted imaging (DWI) sequences were

TR/TE = 1,500,000/22/5. Multislice axial scans were collected with a 5-cm field-of-view and data matrix of 256 × 256, resulting in a 0.195 mm in-plane resolution, slice thickness of 1 mm. T1w sequences were analyzed by calculating the slope of signal changes in multiple scans before and after contrast agent injection. A linear curve was fitted to the dynamic scan intensities at each pixel in the volume of interest revealing the rate of wash-in of contrast agent. For T2w and T1w scan analysis, the Gaussian mixture model with three Gaussian probability density functions was applied to model variety of intensities. Hyperintensities were quantified by including voxel above a segmentation threshold defined as intersection between the 2nd and 3rd Gaussian fit. To remove small-disconnected noise clusters, neighboring pixel connectivity (4-connected) was checked and pixel-cluster smaller than a minimal area was removed as noise. Quantification of apparent diffusion coefficient (ADC) maps was performed by applying a Gaussian fit to the DWI values and defining the mean μ and standard deviation σ values. $\mu \pm 2\sigma$ was used as threshold for "low" and "high" ADC regions (Figure 1(a) to (c), right panels).

Intracranial pressure measurement and Evans blue application

For intracranial pressure (ICP) experiments, anesthesia was induced by ketamin/xylazin injection (0.8 and 0.3 mg/kg b.w., respectively) and maintained by isoflurane (0.8%) via a mask. The ICP probe (ø = 1.33 mm, parenchymal ICP monitoring catheter – 1104B, Camino, Integra NeuroSciences, San Diego, CA, USA) was inserted to a depth of 2.2 mm from dura through a bur hole at 4 mm posterior and 3 mm lateral to bregma (Brain Maps, 1st Edition, L.W. Swanson, Elsevier). ICP values were recorded using a Camino monitor (SPM-1), noted every 10–15 min and stored on computer disk. Photothrombotic stroke was induced ipsilaterally after obtaining a stable ICP baseline for at least 45 min and recordings continued for up to 10 h. A time period of 10–15 min with averaged datapoints of six animals was used for statistical comparison. After the experiment, 2% Evans blue solution (0.2 ml/ 100 g b.w.; Sigma-Aldrich, St Louis, MO, USA) was injected intravenously and 30 min later photographs of the brains were taken after sacrificing the animals.[19,20]

Intrahippocampal recordings

Continuous intrahippocampal field potential recordings were performed using a DSI telemetric system (CA-F40 transmitter, Data Sciences International, St. Paul, MN, USA). Under deep anesthesia (see ICP experiments), three holes were drilled into the rat skull. A teflon-coated platinum iridium wire (ø = 33 µm, Science Products, Hofheim, Germany), soldered to the DSI transmitter, was inserted 2.5 mm lateral, 3.5 mm posterior from bregma to 2.2 mm below dura into the right hippocampal CA1 region (Brain Maps, 1st Edition, L.W. Swanson, Elsevier). The inserted wire was stabilized laterally with a screw (4.5 mm lateral, 5 mm posterior from bregma) and fixated with bone cement. The second electrode was connected to a screw and placed as epidural reference above the left cerebellum (4.5 mm lateral, 5 mm posterior). The transmitter was implanted subcutaneously above the vertebra. Rats were left to recover for four days and baseline recordings were performed for 24–48 h pre- and up to nine days after stroke induction.

Seizures were detected using a "home-made" seizure detection algorithm as described.[23] Recorded data were band-pass filtered (2–100 Hz) and fed to an artificial neural network, which identified characteristic activity (>5 s) patterns as seizures.[24] To examine the effect of stroke on the signal spectral components, we computed the relative power of each 2 s segment in different frequency bands (in Hz): Theta: 3–8, Alpha: 8–12, Beta 1: 12–20, Beta 2: 20–40, Gamma 1: 30–45, Gamma 2: 55–75, Gamma 3: 75–100.[25] To ignore variability imposed by the circadian rhythm, the frequency features were averaged over 24-h periods, focusing on the activity during the 24-h pre-stroke, and during hours 2–26 and 146–170 post-stroke.

Ex vivo recordings

Parasagittal hippocampal slices were prepared as described[20] and superfused with ACSF (in mM: 129 NaCl, 21 $NaHCO_3$, 1.25 NaH_2PO_4, 1.8 $MgSO_4$, 1.6 $CaCl_2$, 3 KCl, 10 glucose, pH 7.4, osmolarity 300 ± 5 mOsm). Extracellular recordings were performed in stratum pyramidale (SP) and radiatum (SR) of CA1 and occasionally also in CA3. Paired stimulus pulses (100 µs duration, 50 ms interstimulus interval (ISI)) were applied every 30 s through bipolar platinum electrodes with 50–60% of the intensity required to induce maximal responses. Electrodes were placed in SR to activate Schaffer collaterals and commissural fibers or in the stratum oriens (SO) to activate pyramidal cell axons and to induce feedback inhibition (Figure 3(a)). The afferent volley amplitudes were measured from SR recordings. Field excitatory postsynaptic potentials (fEPSP) were analyzed by measuring the slope between 20 and 80% of its maximal amplitude. For input–output analysis, we normalized the output (afferent volley, fEPSP and population spike (PS) amplitudes) by dividing the suprathreshold amplitude with the amplitude of threshold intensity required to evoke a PS. In paired pulse experiments, five pulses were averaged for

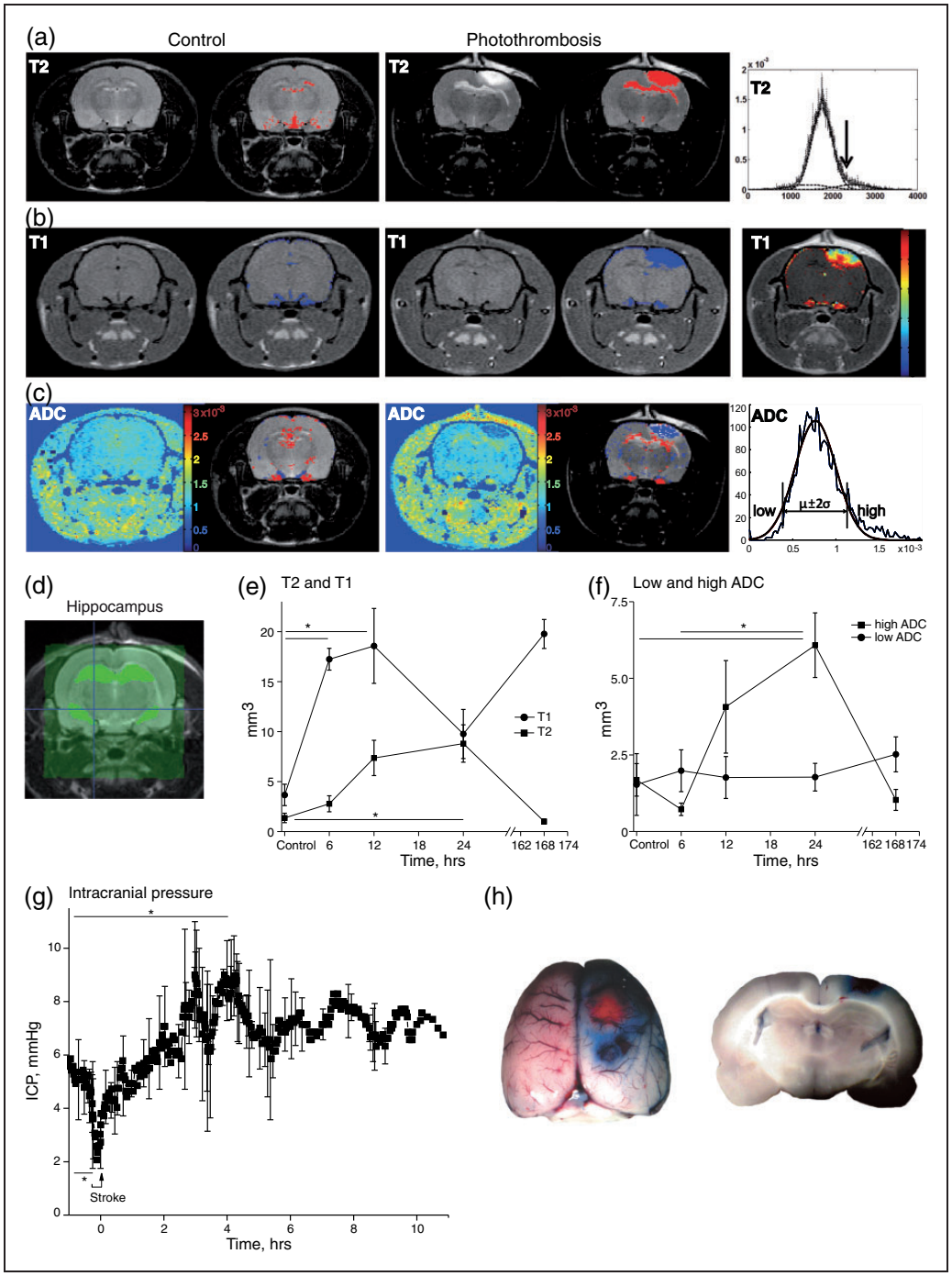

Figure 1. Spatiotemporal quantification of hippocampal BBB breakdown and edema formation following cortical PT. (a–c) T2w, contrast enhanced-T1w scans and ADC maps were acquired from control and PT-treated animals using MRI. Right panels display analysis methods for identifying abnormal intensities. (a, b) Hyperintense areas are mainly displayed in the photothrombotic lesion and the underlying hippocampus (T2 red, T1 blue overlay). (c) ADC map analysis differentiates between low ADC (blue) associated with cytotoxic edema and high ADC indicating vasogenic edema (red). (d) Scans were segregated for specific hippocampal region analysis. (e, f) Spatiotemporal quantification of abnormal intensities in the ipsilateral hippocampus is displayed (controls (C) and 6 h n = 4, 12 and 24 h n = 6, D7 n = 2). Early increase in T1w scans indicating BBB leakage precedes T2w signal enhancement (Figure 1(e); one-way ANOVA (ANOVA) with Games-Howell post hoc test: T1: $p = 0.007$, post hoc: C vs. 6 h $p = 0.001$, C vs. 12 h $p = 0.048$; T2: $p = 0.011$, post hoc: C vs. 24 h $p = 0.048$). ADC maps confirm a strong vasogenic edema (high ADC: ANOVA: $p = 0.02$, post hoc: C vs. 24 h $p = 0.041$, 6 vs. 24 h $p = 0.018$), but no cytotoxic edema in the hippocampus. (g) Cortical PT leads to a significant increase of 74% in intracranial pressure within a few hours (n = 6, paired t-test: $p = 0.003$). (h) Evans blue extravasation confirms BBB breakdown surrounding the lesion and mildly in the underlying hippocampus.

analysis. To induce long-term potentiation (LTP), we used three trains of 40 pulses applied at 100 Hz with an inter-train interval of 40 s.[26] Slices were selected according to successful LTP induction in PS (>5% potentiation, 35–45′ after induction).[27]

Data acquisition and analysis

Signals were amplified (SEC-10L, NPI, Tamm, Germany), filtered at 3 kHz, displayed on an oscilloscope, digitized on-line (CED-1401, Cambridge, UK), and stored for off-line analysis using Spike 2v6.09 (CED-1401, Cambridge, UK). Custom-made scripts (MATLAB R2010a for Windows) were used for signal analysis. Differences between control and treated slices were determined by type of distribution. Gaussian distribution was estimated by use of the Shapiro–Wilk-test and if normally distributed significance was determined using either ANOVA or Student's t-test. For non-parametric statistics either Friedman or Kruskal–Wallis test (KW), or Wilcoxon Rank or Mann–Whitney-U (MW) test were used. Post hoc analysis was subsequently done including Bonferroni correction. For comparing event incidences, Chi-square test was used. Data are represented as mean values ± SEM. $p < 0.05$ was taken as significance level.

Real-time polymerase chain reaction and microarrays

Total RNA from dissected hippocampi was isolated using the TRIzole reagent (Invitrogen, CA, USA) as described.[18] RNA quality was determined by using the Agilent 2100 Bioanalyzer (Agilent Technologies, CA, USA). cRNA samples were prepared and hybridized to Rat 2.0 ST Arrays (Affymetrix, CA, USA) according to company protocols. Data were normalized as described[18] and gene ontology analysis was based on previous transcriptome studies.[18,28] The expression levels of selected sets of genes were obtained from microarray analysis (Kim SY et al., in preparation). Quantitative reverse transcriptase-polymerase chain reaction (qPCR) with CFX 96 detection system (BioRad, CA, USA) was used to determine the levels of mRNA expression. We used qPCR Miner program to analyze qPCR data.[29] The level of Rplp mRNA was used as reference. Primer sequences are as following: Rplp, 5′-ATCTACTCCGCCCTCATCCT-3′ and 5′-GCAGATGAGGCTTCCAATGT- 3′; rGFAP, 5′- AGAAAACCGCATCACCATTC-3′ and 5′- TCC TTAATGACCTCGCCATC-3′; Kcnj3, 5′-GTGGCG TTGGAACCTCTT TA-3′ and-5′ACATGGGCTTT GTTCAGGTC-3′; Gabrg1, 5′-ACTTCGGTATCCCC AGGTCT-3′ and 5′-CATCTTCCCCTTGAGGCATA-3′; Gabrb2, 5′-GGGCTACTTTGGGATTTGGT-3′ and 5′-CCTCCGAAATCTGGTCTCAG-3′. The data are presented as normalized to sham-operated controls (Rose Bengal or light exposure only).

Results

Hippocampal BBB dysfunction and ICP increase precede vasogenic edema shown by MRI

MRI scans conducted repeatedly under low-level isoflurane anesthesia (6, 12, 24 h and seven days, Figure 1(a) to (f)) showed a clear ischemic core surrounded by perilesional edema that developed within 24 h following photothrombotic stroke similar to previous reports.[19] T2w images (Figure 1(a)) displayed abnormal signal hyperintensity in the lesion core and perilesional brain regions, including the hippocampus, sometimes in both hemispheres (red overlay), indicating higher water content. Contrast enhanced-T1w scans demonstrated areas of BBB leakage (Figure 1(b), blue overlay), strongest in the peri-ischemic region. ADC maps were calculated to estimate vasogenic (red) and cytotoxic edema (blue overlay). As expected, in the lesion core cytotoxic edema dominated while in the underlying, BBB-disrupted hippocampus mostly vasogenic edema was present (Figure 1(c)). Analysis of signal change over time in the segregated ipsilateral hippocampus (Figure 1(d)) revealed a maximal volume of T1w contrast enhancement within 6–12 h after initiating the photothrombotic lesion. This change was followed (at 24 h) by a significant increase in hippocampal volume with T2w abnormal signal (Figure 1(e); one-way ANOVA (ANOVA) with Games-Howell (GH) post hoc test: T1: $p = 0.007$, post hoc: C vs. 6 h $p = 0.001$, C vs. 12 h $p = 0.048$; T2: $p = 0.011$, post hoc: C vs. 24 h $p = 0.048$). ADC maps were consistent with changes in T2w signal, revealing a significant increase in apparent vasogenic edema (''high ADC'') (but not cytotoxic edema) at 24 h (Figure 1(f); ANOVA: $p = 0.02$, post hoc: C vs. 24 h $p = 0.041$, 6 vs. 24 h $p = 0.018$). No significant differences in MR signal were detected in the contralateral hippocampus compared to controls (data not shown). These results suggest early increase in vessels' permeability followed by increased water content within the ipsilateral hippocampus with no apparent irreversible cellular damage.

BBB dysfunction and related vasogenic edema are often associated with increased ICP, which in turn may impact cerebral perfusion. For continuous recording of ICP before and after stroke induction, we used an ICP probe inserted above the hippocampus, ipsilateral to the photothrombotic insult (Figure 1(g), n = 6). ICP baseline values of 5.3 mmHg (60 to 30 min before PT) were consistent with reported values.[30,31] ICP dropped by 48.2% during PT (baseline (n = 19 data points) versus stroke induction (2.6 mmHg, −11 to

0 min, n = 9 data points), paired t-test: $p = 0.002$), then increased significantly by 74% within 4 to 5 h after the insult to a mean of 9.3 mmHg (n = 6, paired t-test: $p = 0.003$) and reached a maximum value of 11.5 mmHg (~4 h 15 min). Following this initial peak, ICP reached a plateau level of ca. 7.1 mmHg with slow oscillating variations of 10.8% over the observation time course of up to 10 h post-stroke. Evans blue injection at the end of the experiment confirmed BBB dysfunction in the perilesional area including the underlying hippocampus (Figure 1(h)).

Post-stroke intrahippocampal recordings

Seizures were recorded within the first nine days after stroke in six out of nine animals (66.7%). Seizures were detected as early as on day 1 (n = 1 rat) and were most frequent at days 3 to 7 after PT. Seizure frequency was variable: in three animals from 28 up to 80 seizures/day were detected, while in three rats no seizures were detected (Figure 2(b)). Frequency analysis was performed in eight animals (one animal was excluded due to technical problems) with and without seizures. Data were averaged for 24 h prior to (−1D), as well as one day (D1) and seven days (D7) after PT. At D1 there was a significant increase in power at the theta band in all animals compared to pre-stroke baseline (repeated measures ANOVA: $p = 0.017$). This was associated with a significant reduction in power at the alpha band in non-seizing rats, but not in rats with seizures (non-seizing: –D1 vs. D1: $p = 0.007$). By contrast, in the beta 2 and gamma 1 frequency range, a reduced power was found at D1 in all animals ($p < 0.001$). Reduction of gamma 1 was more prominent at day 1 in seizing compared to non-seizing animals and extended to day 7 in gamma 2 and 3 (t-test: gamma 1: $p = 0.029$, gamma 2: $p = 0.048$, gamma 3: $p = 0.025$).

Hippocampal CA1 network activity in BBB-disrupted hippocampal slices

We have recently reported the generation of epileptiform episodes (EE), which evolved into spontaneous SDs in slices from animals exposed to PT.[20] These experiments were performed in the presence of extracellular solution mimicking the electrolyte composition of serum. Here, we expanded these observations to slices in which a physiological ACSF was used. Recordings were performed in CA1 in response to paired pulse stimulation of the stratum radiatum (SR) in naive animals, at D1 and D7 after PT (Figure 3(a)). At D1 multiple population spikes were evoked in 20.7% of slices, significantly more often than in control slices (n = 11 of 53 slices/18 animals vs. 1.8%, n = 1 of 55/21; Chi-square: $p = 0.003$; Figure 3(a) and (b)). At D7 multiple PS occurrence was similar to that found in controls (6.7%, n = 3 of 45/14).

EEs occurred spontaneously or were evoked during repetitive stimulation (0.033–100 Hz) and could evolve into SDs characterized by a large negative DC potential shift (Figure 3(c) and (d)). SDs were observed more often at D1 after PT compared to D7 or controls (D1: 23 of 53 slices; D7: 4/45; controls: 4/55, Chi-square: $p = 1.4 \times 10^{-6}$). Notably, in most control or D7 slices (each: n = 3 of 4), SDs were triggered during LTP or depotentiation stimulation protocols (Figure 3(e)). Spontaneous SDs were recorded in 2 out of 53 slices at D1 but never in control or D7 slices.

EEs were defined as prolonged (>1 s), mostly negative field potential shifts with overriding action potentials (Figure 3(f)). At D1 EEs were observed in 75.5% of slices (n = 40/53), significantly more often than in D7 or control slices (Figure 3(g); Chi-square: $p = 3.1 \times 10^{-6}$). By careful analysis of in average 2 h (7397 s) of recording, we observed at D1 > 10 EEs (>1 min interval in-between events) in 14 slices (26.4%), 1–5 EEs in 39.6% and 6–10 EEs in 9.4% of slices. At D7 the number of slices with EEs declined to 46.7% (n = 21/45), with only two slices (4.4%) showing > 10 EEs (1–5 events = 28.9%; 6–10 events 13.3%). In slices from control rats, EEs (never more than 5) were observed in 27.3% of slices (n = 15/55). EE amplitude was also significantly larger at D1 compared to D7 (0.7 ± 0.069 mV (μ±SEM), n = 255 compared to 0.4 ± 0.059 mV, n = 100, Figure 3(h); KW: $p = 0.00037$). No difference between groups was found in EE duration. At D1 EE amplitude was affected by subsequent stimulation protocols with different frequencies and was 0.8 ± 0.087 mV (n = 179) at 0.033 Hz, declined to 0.52 ± 0.13 mV (n = 64) after 100 Hz stimulation, and to 0.28 ± 0.07 mV (n = 12) after 1 Hz depotentiation protocol (Figure 3(i), KW $p = 1.7 \times 10^{-6}$).

Input–output relationships and paired stimulation suggests disinhibition within CA1

To further characterize network hyperexcitability in the BBB-disrupted hippocampus, we next analyzed input–output relations in CA1, while stimulating the SR or SO. Recordings were performed in SR and SP (see scheme Figure 3(a)). Slices were separated into groups depending on EE occurrence. Normalized afferent volley amplitude, indicating presynaptic excitability, was not altered on D1 but increased at D7 (Figure 4(a), for fold threshold input of 1.5–3 and 5, KW: $p < 0.05$). Population spike amplitude was also larger for intermediate stimulation intensities at D7 compared to D1 and control (Figure 4(b), D7 vs. C: for 2–3 and D7 vs. D1 for 2.5: KW $p < 0.05$), whereas no differences

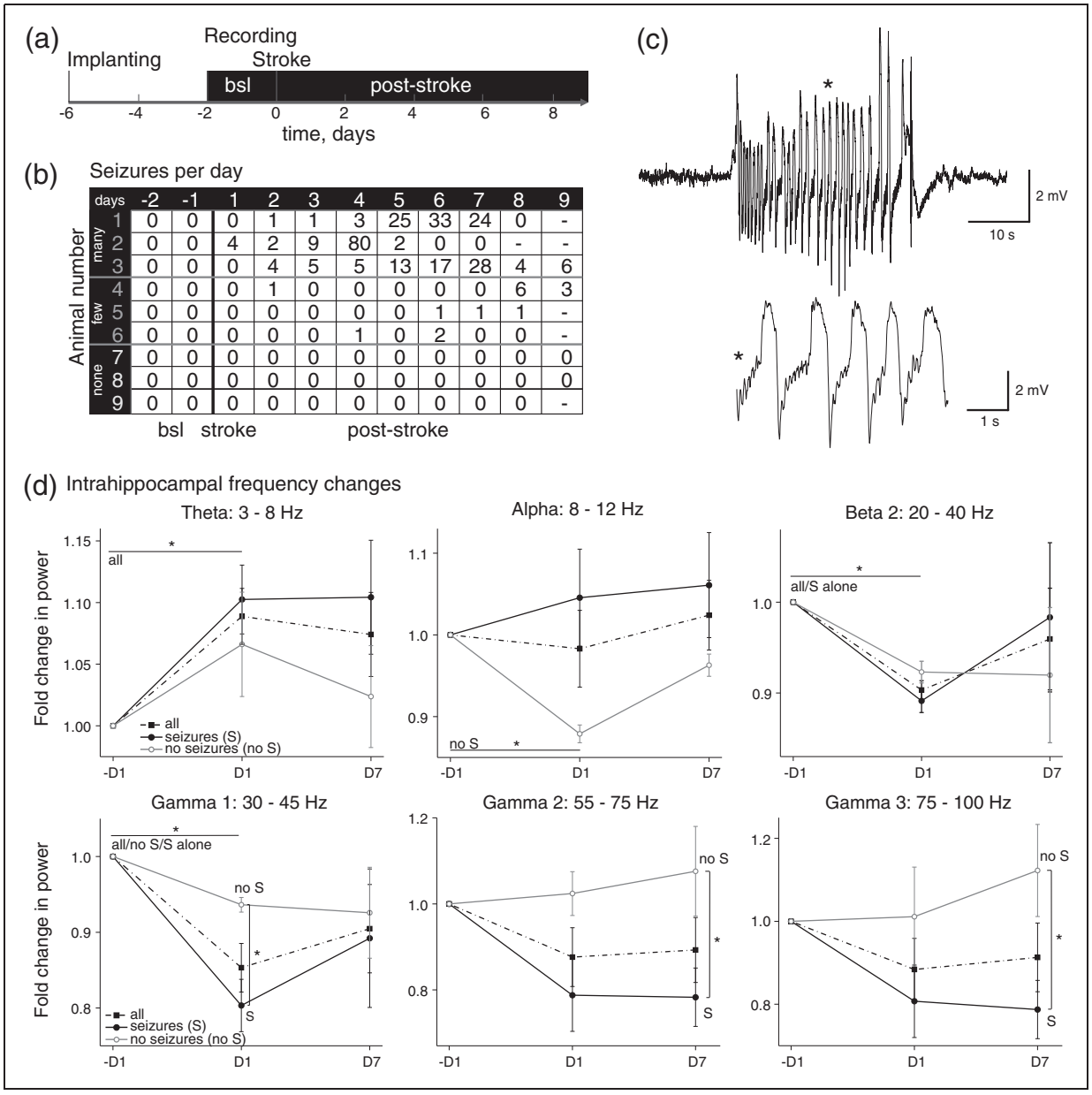

Figure 2. Early seizure onset and gamma to theta shift in post-stroke intrahippocampal field potential recordings. (a) Scheme of electrode implanting and recording time course. (b) Table displays numbers of seizures per day for each animal (n = 9). Note, that there are three groups of animals presenting with many, few or no seizures, respectively. (c) Example traces of a representative hippocampal seizure. (*) Zoom into the seizure. (d) Power analysis of different frequency bands from background activity for D1 and D7 post-stroke compared to pre-stroke (−D1). Graphs include analysis of eight animals and a separation into animal groups presenting with seizures (S, n = 5) or without seizures (no S, n = 3). Theta power was increased at D1 compared to –D1 for all animals, whereas non-seizing animals alone presented lower power at the alpha band (repeated measures ANOVA: 3–8 Hz: all: $p = 0.017$; 8–12 Hz: non-seizing: $p = 0.007$). At 20–40 (beta 2) and 30–45 Hz (gammma1), power was decreased for all animals at D1, partially for seizing or non-seizing animals alone as well (20–40 Hz: all: $p = 0.001$, S: $p = 0.0001$; 30–45 Hz: all: $p = 1 \times 10^{-5}$, S: $p = 0.001$, no S: $p = 0.033$). For higher gamma frequencies, power of seizing animals was strongly diminished compared to non-seizing animals (D1: 30–45 Hz: t-test: $p = 0.029$; D7: 55–75 Hz: $p = 0.048$; 75–100 Hz: MW: $p = 0.025$).

were found between D1 and controls. No significant differences between groups were found in fEPSP slopes (data not shown). These results suggest a change in fEPSP-PS (ES) coupling, which relates to postsynaptic ion channel abundance, processes like dendritic integration or inhibition (Figure 4(c)). Indeed, when PS amplitudes were plotted against fEPSP slopes, the ES-coupling was augmented at D7

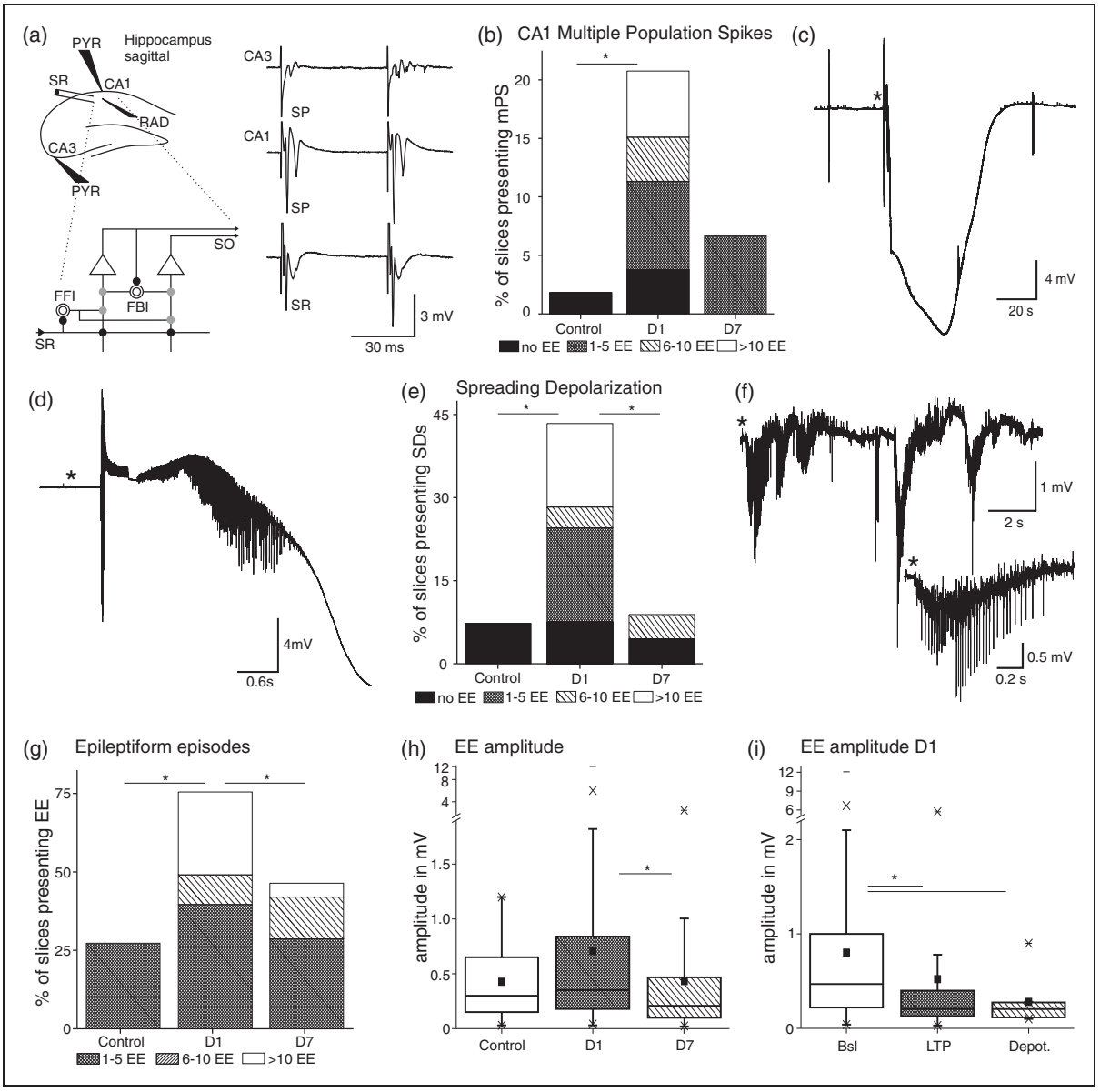

Figure 3. Ex vivo field potential recordings in hippocampal slices present several features of a hyperexcitable network predominantly at D1 post-stroke. (a) Scheme of a sagittal hippocampal slice and electrode positions. Stimulation was done in stratum radiatum (SR) and field potentials were recorded in CA3 stratum pyramidale (SP), CA1 SP (PYR) and SR (RAD). Detail below displays a scheme of the local circuit interactions. Schaffer collaterals input in SR excites (black full circle) pyramidal cells (triangle), whose output projects to SO. Schaffer collaterals activate also interneurons (open circles) for feedforward inhibition (gray full circle, FFI). Axon collaterals from pyramidal cells project to interneurons for feedback inhibition (FBI; scheme modified from: Buhl E and Whittington M. Local Circuits. In: Andersen P et al. (eds). *The hippocampus book*. Oxford University Press, New York, NY, 2007, p.300). Traces on the right panel display examples of multiple population spikes (mPS) and field excitatory postsynaptic potentials (fEPSP) in all recording sites at D1. (b) mPS occurred significantly more often at D1 compared to control (C n = 1 of 55 slices/21 animals, D1 n = 11 of 53/18, overall Chi-square: $p = 0.003$). Bar graphs of Figure 3(b), (e), and (g) were subdivided with regard to the amount of EE slices experienced during recordings lasting on average 2 h. (c) Example of a spreading depolarization (SD) in CA1 SP at D1 during baseline stimulation (0.033 Hz). (d) (*) Zoom in of an epileptiform discharge preceding the SD. (e) Occurrence of SDs, which appeared significantly more often at D1 compared to D7 and controls (C n = 4 of 55/21, D1 n = 23 of 53/18, D7 n = 4 of 45/14; Chi-square: $p = 1.4 \times 10^{-6}$). (f) Trace of a spontaneous epileptiform episode in CA1 SP at D1 post-stroke with a zoom in (*). (g) Occurrence and amount of EE were significantly larger in slices from D1 (C n = 15 of 55, D1 n = 40 of 53, D7 n = 21 of 45; Chi-square: $p = 3.1 \times 10^{-6}$). (h) Amplitudes of EE were larger at D1 compared to D7 including all recordings (D1 n = 255 events (mean $\mu \pm$SEM = 0.7 ± 0.069 mV), D7 n = 100 ($\mu = 0.4 \pm 0.059$ mV); KW: $p = 0.00037$). (i) Within D1 amplitudes of EEs declined with ongoing stimulation protocols (baseline: n = 179 ($\mu = 0.8 \pm 0.087$ mV), LTP n = 64 ($\mu = 0.52 \pm 0.13$ mV), Depot. n = 12 ($\mu = 0.28 \pm 0.07$ mV); KW $p = 1.7 \times 10^{-6}$).

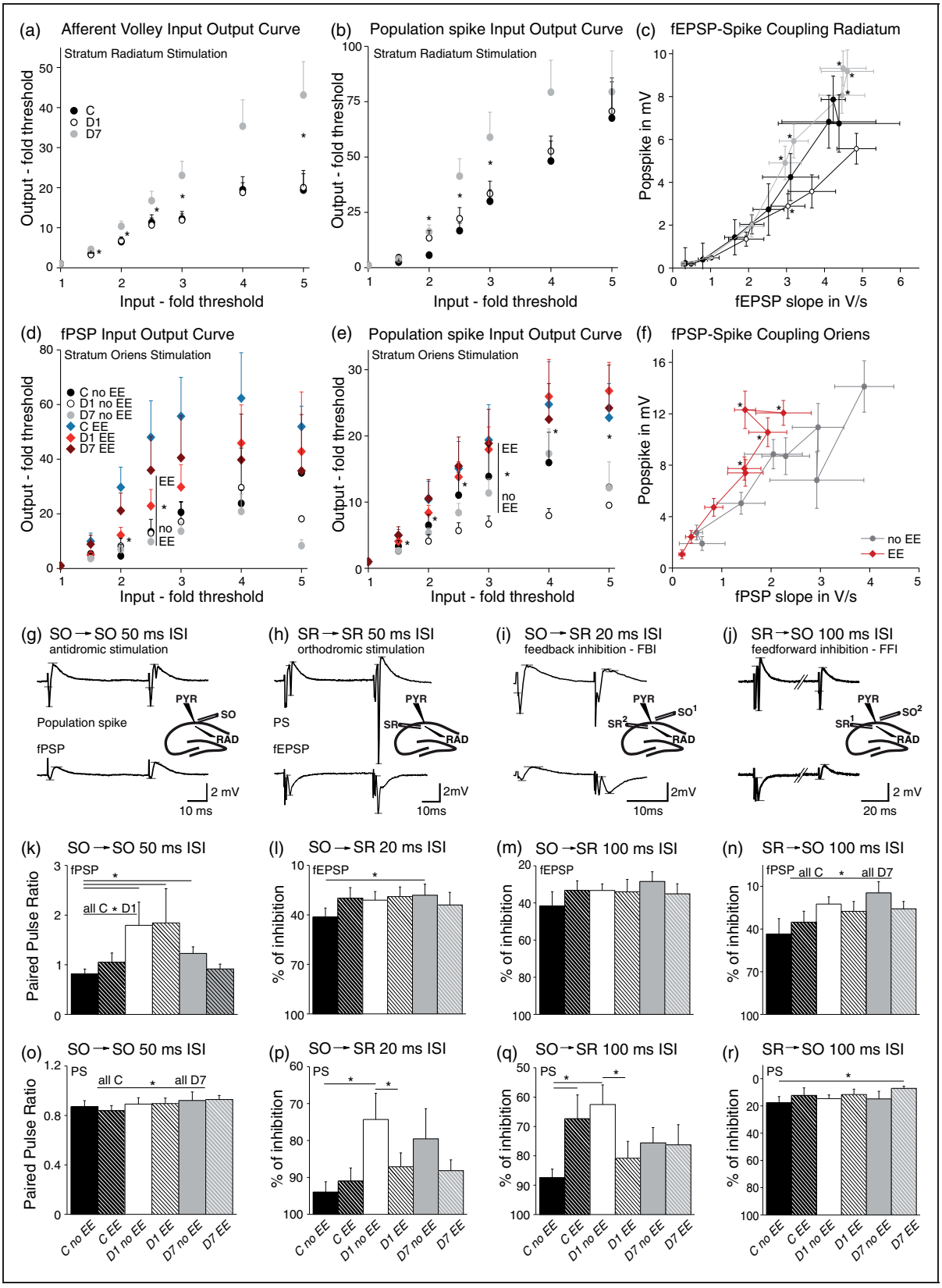

Figure 4. Increased input–output curves, fEPSP-spike (ES) coupling, and decreased feedback as well as feedforward inhibition in CA1 post-stroke. During antidromic stimulation, BBB-disrupted slices revealed increased paired pulse ratios and larger input–output curves, dependent on epileptiform activity. (a) Slices from D7 showed larger afferent volley amplitudes in SR recordings, indicating a

(continued)

slices (for 2.5–7: KW $p < 0.05$; MW post hoc: 2.5–7: D1 vs. D7; 2.5: C vs. D7 and 4: C vs. D1 $p < 0.0167$). By contrast, coupling between afferent volleys and fEPSP displayed no alteration in stroke animals, although afferent volleys had larger amplitudes at D7 compared to no significant changes in fEPSP amplitudes (data not shown).

We next analyzed SO-induced antidromic responses resulting from activation of pyramidal cell axons, which run within the alveus towards the subiculum and the fimbria fornix. SO stimulation induces via axonal collaterals GABAergic synaptic inhibition in CA1[32] and results in positive field potentials (fPSP) in the SR (Figures 3(a) and 4(g)). Interestingly, slope amplitudes were larger for intermediate stimulation intensities in slices with EEs, independent of treatment (Figure 4(d); for 2–2.5, EE vs. no EE: MW $p < 0.05$). Population spikes were also larger in slices with compared to those without EEs (Figure 4(e); for 1.5–5, MW $p < 0.05$). Because changes in ES-coupling for SR stimuli could either be due to changes in dendritic excitability or due to disinhibition, we tested whether there was an altered coupling between the amplitude of SO-evoked PSs and fPSPs. Indeed, slices with EEs showed increased fPSP-spike coupling compared to slices without EEs (Figure 4(f); for 3–7, MW $p < 0.05$), suggesting that reduced GABAergic inhibition within CA1 underlies hyperexcitability.

We then tested for paired pulse ratio in response to SR stimulation with 50 ms ISI. We always observed paired pulse facilitation with no difference between post-stroke slices and controls, suggesting a similar release probability of presynaptic vesicles (Figure 4(h)). In contrast, SO-induced fPSPs revealed a significant increase in paired pulse ratio at D1 compared to control (Figure 4(g) and (k); all C vs. D1: MW $p = 0.027$), while the ratio between PS amplitude was not affected. At D7 paired pulse ratio of PS and fPSP amplitude was increased in slices from treated animals compared to controls (Figure 4(o); C vs. D7: MW $p = 0.045$; Figure 4(k); C no EE vs. D7 no EE: MW $p = 0.032$). These experiments suggested a reduced GABAergic inhibition in the BBB dysfunctional hippocampus.

To further test for functional feedback inhibition, we paired SO and SR stimulation with an inter-stimulus interval of 20 ms (for $GABA_A$-mediated inhibition). This protocol stimulates CA1 pyramidal cell axonal collaterals that activate interneurons, which in turn inhibit CA1 pyramidal dendrites (circuitry in Figures 3(a) and 4). Vice versa, for induction of feedforward inhibition, SR preceded SO stimulation to activate – via Schaffer collaterals in SR – interneurons, which inhibit the incoming signal in dendrites of CA1 pyramidal cells (Figure 3(a)). The degree of inhibition was calculated as the ratio of the inhibited and the non-inhibited signal from the same stimulation site. In slices from controls, response to SR stimulation was significantly smaller compared to SR stimulation only when it followed SO stimulation, due to activation of GABAergic interneurons by SO stimulation (Figure 4(h) to (i)). At D1 PS and at D7 fEPSP amplitudes were significantly enlarged, suggesting a decline in feedback inhibition (Figure 4(p); PS MW: C no EE vs. D1 no EE: $p = 0.014$; Figure 4(l); fEPSP: C no EE vs. D7 no EE: $p = 0.041$). An increase in PS amplitude at D1 was also observed when SO-SR stimulus interval was 100 ms, suggesting that $GABA_B$-mediated late inhibition may also be affected (Figure 4(q): C no EE vs. D1 no EE: $p = 0.009$). We observed stronger

Figure 4. Continued
greater number of activated presynaptic fibers (C n = 16 slices/7 animals, D1 n = 33/14, 7d n = 27/8; for fold threshold input of 1.5–3 and 5, KW: $p < 0.05$). (b) Population spike amplitudes were increased at D7, too (C n = 18/8, D1 n = 33/14, D7 n = 27/8; for 2–3-fold threshold: C vs. D7 and for 2.5: D1 vs. D7: KW $p < 0.05$). (C) ES-coupling was enhanced at D7 compared to a smaller coupling at D1 (for 2.5–7: KW $p < 0.05$; MW post hoc: 2.5–7: D1 vs. D7; 2.5: C vs. D7 and 4: C vs. D1 $p < 0.0167$). (d–f) For antidromic stimulation (SO), amplitudes of field postsynaptic potentials (fPSP) and population spikes as well as the fPSP-spike coupling were increased in slices displaying EE independent of their treatment (PS: for 1.5–5: all EE (n = 28/18) vs. all no EE (n = 15/11): MW $p < 0.05$; fPSP: for 2–2.5, MW $p < 0.05$; fPSP-spike coupling: for 3–7, MW $p < 0.05$). (g–j) Example traces of recordings during paired pulse stimulation with small schemes presenting the stimulation and recording sites. Horizontal lines in traces mark points between which amplitudes and slopes (fEPSP) were calculated. (g–h) Antidromic and orthodromic paired pulse stimulation (50 ms ISI) was done for investigating short-term plasticity. (i, j) Alternating stimulation, where an SO stimulus was followed by an SR stimulus and vice versa, was performed for testing for feedback and feedforward inhibition, respectively. (k, o) Paired pulse ratio of SO stimulation was increased in D1 and D7 post-stroke slices for fPSP and in D7 slices for PS (fPSP: all C n = 13/8, D1 n = 21/11; MW: p = 0.027; C no EE n = 7/6, D7 no EE n = 10/5; MW $p = 0.032$; PS: C n = 10/5, D7 n = 17/7, MW: $p = 0.045$). (l, p) $GABA_A$-mediated feedback inhibition (20 ms ISI) was declined at D1 for PS and at D7 for fEPSP in slices without EE. Slices from D1 with EE displayed stronger inhibition than without EE in PS (PS: C no EE n = 8/6, D1 no EE n = 6/5, D1 EE n = 17/11; MW: no EE: C vs. D1: $p = 0.014$; D1 no EE vs. D1 EE: $p = 0.042$; fEPSP: C no EE n = 8/6, D7 no EE n = 10/5, MW: no EE: C vs. D7: $p = 0.041$). (m, q) $GABA_B$-mediated feedback inhibition (100 ms ISI) of PS was smaller in D1 slices without EE and in controls with EE compared to controls without EE. D1 with EE revealed stronger inhibition than without EE (C no EE n = 7/6, C EE n = 5/4, D1 no EE n = 7/6, D1 EE n = 14/9; MW: no EE: C vs. D1: $p = 0.009$; C no EE vs. EE: $p = 0.028$; D1 no EE vs. EE: $p = 0.029$). fEPSP presented no differences. (n, r) $GABA_B$-mediated feedforward inhibition was lowered at D7 for fPSP and PS (fPSP: C n = 14/8, 7d n = 17/7, MW: $p = 0.035$; PS: C no EE n = 7/6, 7d EE n = 7/5, MW: $p = 0.049$).

disinhibition in treated slices without compared to slices with EE, which we cannot explicitly explain. Interestingly, effects of SO stimulation on fEPSPs were generally weaker compared to PSs (Figure 4(m)), indicating a stronger reduction in perisomatic feedback inhibition.

To test for feedforward inhibition, we first stimulated in the SR before the SO (20 ms ISI). No significant alterations were found in slices from PT-exposed rats, suggesting that $GABA_AR$-mediated disinhibition mostly involves feedback pathways (data not shown). At stimuli interval of 100 ms, fPSP and PS amplitudes were increased at D7, suggesting decreased $GABA_B$-mediated feedforward inhibition (Figure 4(j, n, r); MW: fPSP: all C vs. D7: $p = 0.035$; PS: C no EE vs. D7 EE: $p = 0.049$).

Impaired long-term plasticity

Activation of astrocytes in the BBB-disrupted cortex[28] and early disinhibition as described here predict impaired synaptic plasticity. Indeed, previous studies described an altered induction of LTP in the peri-ischemic cortex.[33,34] We thus induced LTP in hippocampal slices from PT-treated rats and controls. In response to stimulation of the Schaffer collaterals, no significant differences were found in the percentage of slices in which stable LTP was induced in both the CA1 (92% of control, n = 36 slices/16 rats; 83% of D1, n = 24/13; 75% of D7 slices, n = 28/12) and CA3 (due to antidromic stimulation) regions (81% of control, n = 16/4; 92% of D1, n = 12/4; 54% of D7 slices, n = 11/3). Interestingly, while potentiation of both fEPSP and PS amplitude was unaltered at D1, PS potentiation was markedly reduced in both CA1 and CA3 at D7, predominantly in slices presenting EE (Figure 5(b): KW $p = 0.03$, post hoc: C no EE vs. D7 EE, $p = 0.0007$; Figure 5(c): planned comparison one-way ANOVA (pANOVA): within groups $p = 0.021$; GH post hoc: 24 h EE vs. 7d EE $p = 0.049$).

The reduction in potentiation at D7 raises the possibility that synaptic paths are already potentiated at this stage. We thus added a depotentiation protocol (1 Hz, 900 stimuli) after induction of a stable LTP.[26] Stable depotentiation (>5%, last 10′) of PS amplitude was measured in most slices from all groups (73% of control, n = 11/8; 62% of D1, n = 13/7; and 63% of D7 slices, n = 8/5). Population spikes in D7 slices with EE showed significantly less LTP and a strong tendency for impaired depotentiation compared to control slices (Figure 5(d), pANOVA $p = 0.049$, GH post hoc: C no EE vs. 7d EE $p = 0.009$), suggesting a bidirectional impaired long-term plasticity in D7 slices with hyperexcitability. Due to frequent occurrence of SDs in treated groups and differentiation into EE subgroups, the number of slices is rather small. Therefore, the observed tendency of the depotentiation data has to be confirmed in future studies.

Molecular analysis supports astrocytic activation and $GABA_AR$ downregulation in the BBB-disrupted hippocampus after PT

The electrophysiological data suggest that in the BBB-disrupted peri-ischemic hippocampus, network excitability is increased, GABAergic inhibition is reduced, and synaptic plasticity is impaired. We therefore investigated gene expression for pathways potentially associated with these modifications. Consistent with previous reports on gene expression changes in the BBB-disrupted neocortex,[18] microarray data from ipsilateral hippocampus confirmed that genes associated with endothelial dysfunction (including the tight junction protein claudin) and transforming growth factor beta (TGFß) signaling molecules (Smad6, Fos, ACE) were upregulated at 12 h after PT with a subsequent decline at D1 (Figure 6(a), $> 1 \approx 2$-fold change). Genes associated with astrocytic transformation (GFAP, Vimentin and S100A) were up-regulated at D1 after PT. GFAP upregulation was confirmed using qPCR (Figure 6(d), Sham vs. D1, t-test: $p = 1.5 \times 10^{-5}$). In contrast to previous studies on the BBB-disrupted neocortex, we could not confirm downregulation of Kir4.1 mRNA, but did find a significant downregulation of the G protein-coupled inward rectifying potassium channel Kir3.1 at D7 (Figure 6(e), Sham vs. D7; $p = 0.025$). In agreement with the physiological data, microarray results confirmed a clear tendency for downregulation of $GABA_AR$-associated genes 12 h after PT (Figure 6(b)). qPCR confirmed a significant reduction of Gabrb2 and Gabrg1 receptor subunits at D1 (Figure 6(f) to (g), Sham vs. D1, MW: Gabrb2 $p = 0.0028$, Gabrg1 $p = 0.018$). No changes were found in the expression of Gabra4 and Gabrd (data not shown), important for tonic inhibition.[35] With respect to impaired LTP induction at D7, it is interesting to note that we did not find significant changes in the expression of AMPA or NMDA receptor-related genes (Figure 6(c)).

Discussion

Cortical strokes present a risk factor for epileptogenesis and associated co-morbidities, including cognitive decline.[2] Using the photothrombotic stroke model we show here, that (1) cortical PT is associated with hippocampal BBB dysfunction and vasogenic edema (in contrast to the cytotoxic edema in the ischemic neocortex) and increase in ICP; (2) The BBB-disrupted hippocampus displayed spontaneous seizures in two-thirds of

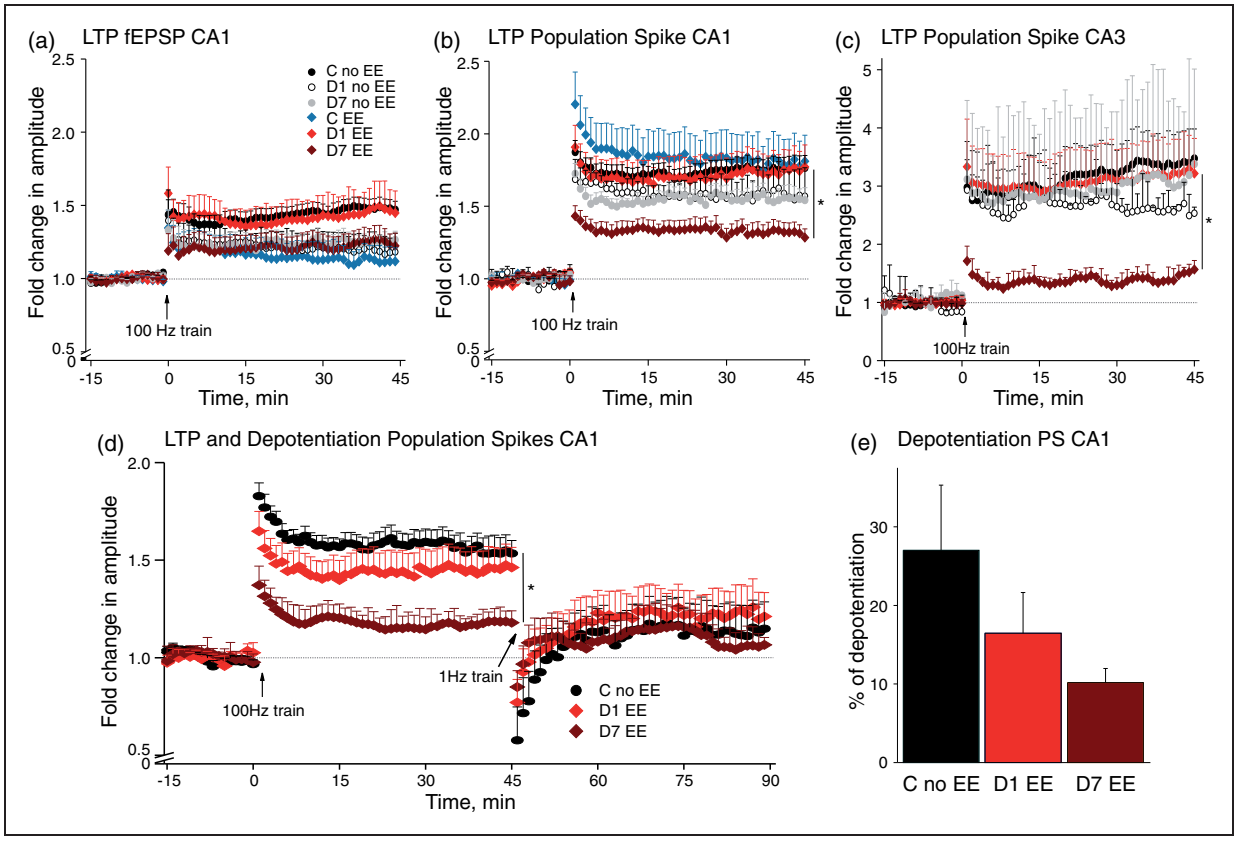

Figure 5. Bidirectional long-term plasticity was disturbed in slices from D7 post-stroke presenting with epileptiform activity. (a) Recordings from the dendritic area of CA1 revealed a modest, but insignificant reduction in LTP for all groups except D1 with EE compared to controls without EE. (b, c) LTP in PS recorded from the somatic area of CA1 and CA3 were strongly diminished in D7 slices with EE ((b): KW $p = 0.03$, C no EE (n = 25/13) vs. D7 EE (n = 11/6), MW post hoc: $p = 0.0007$; (c): planned comparison one-way ANOVA (pANOVA): within groups $p = 0.021$; Games-Howell (GH) post hoc: 24 h EE (n = 8/3) vs. 7d EE (n = 4/3) $p = 0.049$). (d, e) Investigations of bidirectional long-term plasticity revealed reduced LTP and a tendency for less ability of depotentiation in D7 slices with EE ((d) LTP: pANOVA $p = 0.049$, GH post hoc: C no EE (n = 8/6) vs. 7d EE (n = 3/3) $p = 0.009$).

animals within the first week. In seizing animals, spectral analysis of hippocampal background activity showed a shift from gamma to theta frequency band; (3) Using ex vivo recordings, we confirmed hippocampal hyperexcitability after PT with SR-induced multiple PSs, epileptiform events and SDs already at D1, whereas facilitated afferent fiber activation and increased ES-coupling were recorded at D7; (4) Paired pulse experiments suggested decreased feedback and feedforward inhibition in CA1; (5) Impaired LTP and depotentiation were observed at D7 in slices with epileptiform events; (6) Molecular analysis confirmed upregulation in TGFß- and astrocyte-related genes and downregulation in $GABA_AR$ subunits.

Cortical PT leads to microvascular injury and BBB dysfunction within the first few hours after PT.[36] We measured ICP increase during the same time window, probably due to the associated influx of water molecules into the extracellular space. Concomitantly, Evans blue extravasation, changes in contrast enhanced-T1w, and T2w MRI scans were all consistent with early BBB dysfunction. While experiments in the open window technique (where there is likely no ICP increase) demonstrate BBB dysfunction in normally perfused brain adjacent to the ischemic lesion,[36] the associated edema and increase in ICP may contribute to facilitate further BBB breakdown in more remote areas, perhaps due to reduced cerebral blood flow. This supports craniotomy as a therapeutic option in ischemic stroke to prevent further BBB opening.[37] Other factors like propagating SDs and seizures, free radicals, and upregulation of MMPs may contribute further to BBB disruption, associated vasogenic edema, and astrocytic activation.[4,38–41] Changes in T2w scans and ADC maps followed those of contrast enhanced-T1w scans, suggesting the importance of contrast enhanced imaging for the identification of BBB damage as an early biomarker of tissue prognosis. The early drop in high ADC at 6 h may reflect "dendritic beading" induced by SDs,[4] which can lead to

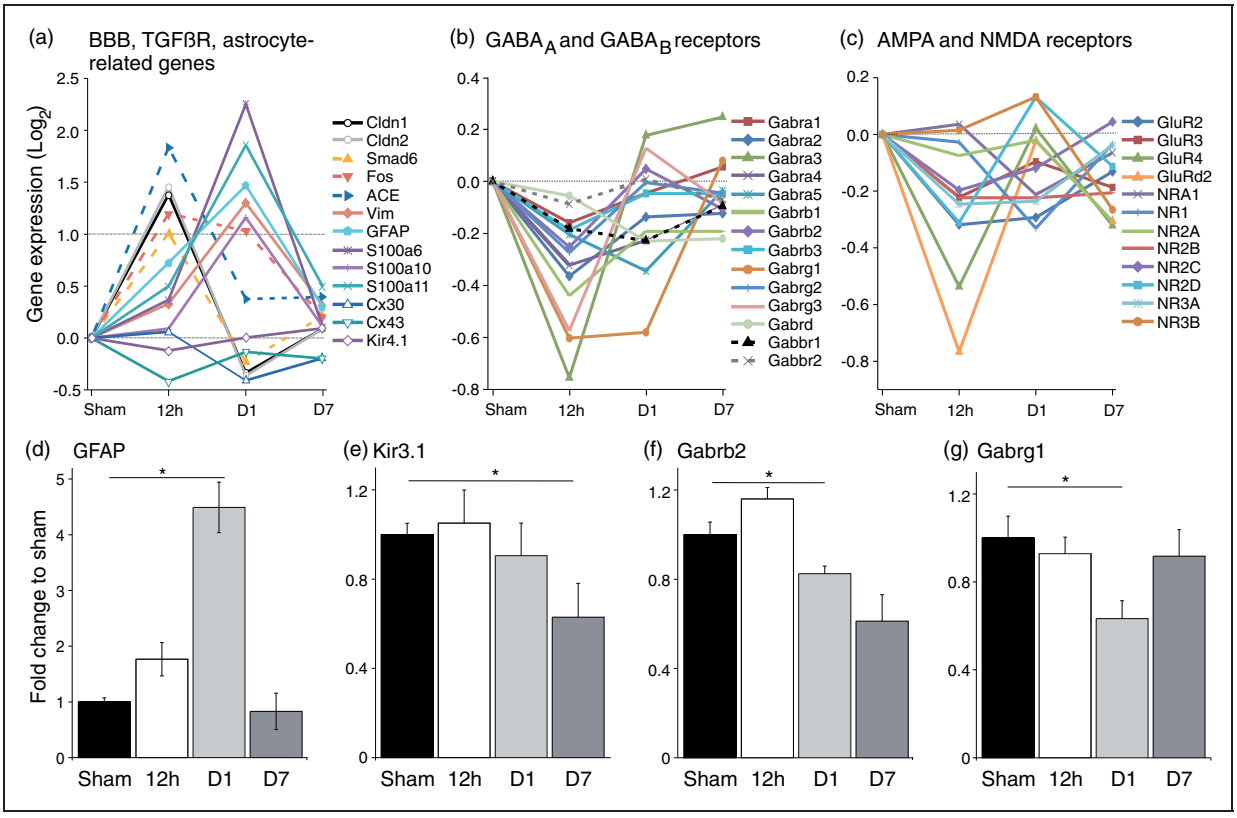

Figure 6. Microarrays and qPCR propose possible underlying causes for network hyperexcitability. (a) Genes associated with tight junctions and TGFß receptor signaling showed increased expression at 12 h post-stroke. Astrocyte-related genes were subsequent upregulated with their peak at D1 (n = 1 at 12 h, D1 and D7 for sham and stroke, respectively). (b) Subunits of $GABA_A$Rs presented as a group a tendential downregulation at 12 h. Subunits of $GABA_B$Rs were not altered. (c) Gene expression of postsynaptic NMDA and AMPA receptors was not affected by stroke. (d) qPCR results revealed at D1 a significant increase in expression of GFAP, indicating astrocytic transformation (Sham (n = 6) vs. D1 (n = 5); t-test: $p = 1.5 \times 10^{-5}$). (e) Gene expression of the G protein-coupled inwardly rectifying potassium channel Kir3.1 was lowered at D7, which is associated with $GABA_B$Rs (Sham (n = 6) vs. D7 (n = 4); t-test: $p = 0.025$). (f, g) Beta2 and gamma1 subunits of $GABA_A$Rs were downregulated at D1 post-stroke (each: Sham (n = 6) vs. D1 (n = 5), MW: Gabrb2 $p = 0.0028$, Gabrg1 $p = 0.018$).

dendritic injury and thereby also contribute to aberrant synaptic plasticity.[42] The on-going increase and slow oscillations in ICP are pointing to a yet unknown dynamic process, where effects of uptake and degradation of serum proteins, variations in perfusion pressure, and dynamic changes at the blood–brain interface may be involved. While we cannot exclude a direct damaging effect due to ICP probe insertion (diameter of 1.33 mm), this is unlikely as ICP baseline values are in line with previous reports,[30,31] and the extent of BBB dysfunction was not different than that observed in experiments with no ICP probe.

Importantly, we found BBB damage preceding the onset of spontaneous seizures in intrahippocampal recordings. These results are consistent with recent recordings from a patient with subarachnoid hemorrhage, in which spontaneous focal seizures were recorded using subdural opto-electrodes, were followed and co-localized with neocortical BBB breakdown shown by MR imaging.[43] It is thus suggested that the extent of microvasculopathy, specifically BBB dysfunction, predicts the occurrence of focal cortical seizures. This is consistent with our studies showing focal neocortical epileptiform activity days after experimental BBB opening or brain exposure to serum albumin.[17,44] Unfortunately, due to technical limitations we could not scan animals with implanted electrodes and could not test whether the large differences found between animals in the number of seizures reflects different susceptibility for BBB dysfunction. Hippocampal seizures were not related to the occurrence of periodic lateralized epileptiform discharges (PLEDs) as the duration of single events was much longer and the recurrence rate lower than those observed in stroke patients or rat focal ischemia.[45,46] Seizing animals experienced a significant shift in on-going background activity from gamma to theta, suggesting ictogenic network modifications. Continuous recordings of background activity and dynamic analysis

of power changes after an insult might therefore serve as predictors of seizures. The observed decrease in gamma band may reflect the susceptibility of fast-spiking inhibitory interneurons to metabolic stress and free radicals[38] and predicts impairment of feedforward inhibition required for the generation of high frequency oscillations.[47,48] Thus, the in vivo monitoring of BBB integrity, ICP, and electrographic activity can all serve as biomarkers indicative of significant, perhaps irreversible, modifications in local brain networks associated with microvascular injury.

Our in vitro recordings confirmed pathological increase in excitability within the peri-ischemic hippocampal network, expressed as SDs and epileptiform discharges. That excitability increase was recorded in vitro under physiological ACSF, denoting it to be due to long-lasting intrinsic modifications and not solely due to transient environmental effects (e.g. increased ICP, reduced blood flow, BBB dysfunction). Interestingly, spontaneous EEs infrequently occurred also in slices from non-treated controls, presumably due to transient inhibitory failure in Wistar rats[49] or due to trauma involved in slice preparation. The occurrence rate and amplitude of EEs were most prominent at D1 after PT, declining at D7. Interestingly, in slices only from D1, EE amplitudes decreased significantly after LTP and even more after the depotentiation protocol, suggesting that high-frequency stimulation potentially reduces uncontrolled network firing. The occurrence of SDs was maximal at D1 and back to control level at D7. Likewise, patients with subarachnoid hemorrhage present their early maximum of SDs in the first two days, preceding the peak of seizure occurrence around day 8,[43,50] consistent with the onset of seizures in our in vivo data. Notably, most SDs were triggered following repetitive stimulation, when oxygen consumption increases and extracellular potassium rises. This could facilitate SD emergence also in remote areas from the core ischemic lesion,[51] when maintenance systems and neural networks are affected. Importantly, the threshold for SD induction and the occurrence of spontaneous SDs are only transiently lowered around D1 and not at D7, consistent with recordings in brain slices from epilepsy patients resected hippocampi and animal models showing increased threshold for SD induction in chronic epilepsy.[4,52,53]

We suggest an early functional GABAergic disinhibition in the BBB-impaired hippocampus around D1 after PT based on the following observations: (1) High-frequency gamma activity, dependent on fast-spiking inhibitory interneurons, was reduced in seizing animals; (2) SR stimulation frequently induced multiple PSs and SO stimulation revealed increased input–output curves and ES-coupling in slices presenting epileptiform activity. Impaired perisomatic inhibition mediated by, e.g. axo-axonic cells, which usually control back-propagating action potentials and are highly vulnerable to metabolic stress,[47,54] may thereby be involved; (3) SO stimulation displayed enhanced-paired pulse ratio. Thus, in addition to impaired perisomatic inhibition, dendrite-targeting inhibition controlling positive fPSPs may be affected as well; (4) Diminished $GABA_{A+B}$-mediated feedback inhibition shown by combined SO-SR stimulation and (5) reduced mRNA expression of $GABA_AR$ subunits support this hypothesis.

We describe changes in the function of the peri-ischemic hippocampal network, lasting for seven days (after BBB permeability was restored), that include: (1) increased afferent volley amplitude to stimulation, suggesting changes in fiber excitability; (2) lower threshold for SR-induced action potential generation and increased ES-coupling. This may be due to changes in intrinsic properties, dendritic morphology, reduced inhibition and excitatory synaptogenesis[55]; (3) diminished functional $GABA_BR$-mediated feedforward inhibition, and (4) limited bidirectional long-term plasticity in slices with epileptiform activity.

For fighting vasogenic edema, albumin uptake into astrocytes is probably essential[40] and seems to involve TGFß signaling leading to alterations in astrocytic properties.[18,56] Our microarray data confirm the involvement of TGFß signaling molecules, like SMAD6, and a subsequent astrocytic transformation in the BBB-disrupted peri-ischemic hippocampus, as previously shown in the cortex in models for BBB dysfunction.[18,28,56] These results are also consistent with studies showing alterations in hippocampal potassium homeostasis after albumin treatment.[20] The cortical astrocytic transformation was also shown to contribute to reduced buffering of glutamate and potassium, leading to their extracellular accumulation in an activity-dependent manner and leading, at least temporarily, to reduction in the spatial specificity of synaptic transmission.[28] Glutamate and GABA could thereby leak from the synaptic cleft and interact with extrasynaptic receptors and presynaptic terminals. The reduced expression of Kir3.1 mRNA indicates reduced sensitivity of $GABA_BR$-mediated signaling enhancing glutamate and GABA release.[57] The augmented potassium accumulation will additionally prolong presynaptic depolarization and increase transmitter release and may cause reduced chloride extrusion from neurons. Interneuronal dysfunction and reduced expression of postsynaptic GABARs can also contribute towards a shift between excitation and inhibition in favor of excitation. Together, these astrocytic-mediated effects on neuronal functions are expected to lower the threshold

for hypersynchronous epileptic discharges and SDs, as well as alter network plasticity.

Our data from LTP experiments present an example for excitation-induced changes in plasticity. Potentiation and depotentiation of PSs were particularly impaired in D7 slices with epileptiform activity. The concomitant reduction in gamma activity recorded in vivo and impaired long-term plasticity in animals presenting epileptiform activity is an interesting characteristic of the affected hippocampal network and may underlie observed cognitive dysfunctions.

In conclusion, the remote and transient opening of the BBB in the hippocampus adjacent to the injured neocortex is associated with reduced inhibition and hyperexcitability of the neuronal network. This is associated with an early and temporary reduction in the threshold for spreading depolarization and epileptiform discharges, and delayed, perhaps lasting changes in plasticity and oscillatory activity, which may contribute to cognitive co-morbidities in patients with focal cortical injury.

Funding

The author(s) disclosed receipt of the following financial support for the research, authorship, and/or publication of this article: This work was supported by German research foundation grant He 1128/19-1 to UH and AF, by the Cluster of Excellence DFG-EXC 257 NeuroCure, the GRK 1123, the EU FP6 grant 602531 "Desire," the European Union's Seventh Framework Program (FP7/2007-2013) under grant agreement n°602102 (EPITARGET) (A.F.), the NIH National Institute of Neurologic Disorders and Stroke (RO1/NINDS NS066005, A.F.), the Israel Science Foundation (A.F.), and the Nova Scotia Health Research Foundation (A.F.).

Acknowledgements

We acknowledge gratefully the technical and organizational assistance of Dr. K. Schulze and Jan-Olliver Hollnagel, for his help with Matlab programming.

Declaration of conflicting interests

The author(s) declared no potential conflicts of interest with respect to the research, authorship, and/or publication of this article.

Authors' contribution

KL: planning and execution of surgery, in vivo measurements, ex vivo electrophysiology and analyses, writing the ms.; LK: development of seizure detection algorithm and analysis of intrahippocampal recordings; SYK: analysis of expression changes; SL: analysis of MRI scans; OP: contributed to MRI and ICP experiments; JFN: contributed to LTP measurements; SS: contributed to electrophysiological control data; DK: planning and supervising the expression analysis, editing the ms.; UH and AF: planning and supervising the experiments and data analysis, writing the ms.

References

1. Herman S. Epilepsy after brain insult: targeting epileptogenesis. *Neurology* 2002; 59(9 Suppl 5): S21–S26.
2. Bladin CF, Alexandrov AV, Bellavance A, et al. Seizures after stroke: a prospective multicenter study. *Arch Neurol* 2000; 57: 1617–1622.
3. Schoknecht K, David Y and Heinemann U. The blood-brain barrier-gatekeeper to neuronal homeostasis: clinical implications in the setting of stroke. *Semin Cell Dev Biol* 2015; 38: 35–42.
4. Dreier JP and Reiffurth C. The stroke-migraine depolarization continuum. *Neuron* 2015; 86: 902–922.
5. Friedman A and Heinemann U. Role of blood-brain barrier dysfunction in epileptogenesis. In: Noebels JL, Avoli M, Rogawski MA, et al. (eds) *Jasper's basic mechanisms of the epilepsies*. Bethesda, MD: National Center for Biotechnology Information (US) Michael A Rogawski, Antonio V Delgado-Escueta, Jeffrey L Noebels, Massimo Avoli and Richard W Olsen, 2012.
6. Tanaka E, Yamamoto S, Kudo Y, et al. Mechanisms underlying the rapid depolarization produced by deprivation of oxygen and glucose in rat hippocampal CA1 neurons in vitro. *J Neurophysiol* 1997; 78: 891–902.
7. Muller M and Somjen GG. Na(+) and K(+) concentrations, extra- and intracellular voltages, and the effect of TTX in hypoxic rat hippocampal slices. *J Neurophysiol* 2000; 83: 735–745.
8. Erdemli G, Xu YZ and Krnjevic K. Potassium conductance causing hyperpolarization of CA1 hippocampal neurons during hypoxia. *J Neurophysiol* 1998; 80: 2378–2390.
9. Fleidervish IA, Gebhardt C, Astman N, et al. Enhanced spontaneous transmitter release is the earliest consequence of neocortical hypoxia that can explain the disruption of normal circuit function. *J Neurosci* 2001; 21: 4600–4608.
10. Vyskocil F, Kritz N and Bures J. Potassium-selective microelectrodes used for measuring the extracellular brain potassium during spreading depression and anoxic depolarization in rats. *Brain Res* 1972; 39: 255–259.
11. Heinemann U and Lux HD. Ceiling of stimulus induced rises in extracellular potassium concentration in the cerebral cortex of cat. *Brain Res* 1977; 120: 231–249.
12. Hinzman JM, DiNapoli VA, Mahoney EJ, et al. Spreading depolarizations mediate excitotoxicity in the development of acute cortical lesions. *Exp Neurol* 2015; 267: 243–253.
13. Strong AJ, Venables GS and Gibson G. The cortical ischaemic penumbra associated with occlusion of the middle cerebral artery in the cat: 1. Topography of changes in blood flow, potassium ion activity, and EEG. *J Cereb Blood Flow Metab* 1983; 3: 86–96.
14. Hossmann KA. Viability thresholds and the penumbra of focal ischemia. *Ann Neurol* 1994; 36: 557–565.
15. Shin HK, Dunn AK, Jones PB, et al. Vasoconstrictive neurovascular coupling during focal ischemic depolarizations. *J Cereb Blood Flow Metab* 2006; 26: 1018–1030.

16. Woitzik J, Pinczolits A, Hecht N, et al. Excitotoxicity and metabolic changes in association with infarct progression. *Stroke* 2014; 45: 1183–1185.
17. Friedman A, Kaufer D and Heinemann U. Blood-brain barrier breakdown-inducing astrocytic transformation: novel targets for the prevention of epilepsy. *Epilepsy Res* 2009; 85: 142–149.
18. Cacheaux LP, Ivens S, David Y, et al. Transcriptome profiling reveals TGF-beta signaling involvement in epileptogenesis. *J Neurosci* 2009; 29: 8927–8935.
19. Stoll G, Kleinschnitz C, Meuth SG, et al. Transient widespread blood-brain barrier alterations after cerebral photothrombosis as revealed by gadofluorine M-enhanced magnetic resonance imaging. *J Cereb Blood Flow Metab* 2009; 29: 331–41.
20. Lapilover EG, Lippmann K, Salar S, et al. Peri-infarct blood-brain barrier dysfunction facilitates induction of spreading depolarization associated with epileptiform discharges. *Neurobiol Dis* 2012; 48: 495–506.
21. Dorr A, Sled JG and Kabani N. Three-dimensional cerebral vasculature of the CBA mouse brain: a magnetic resonance imaging and micro computed tomography study. *Neuroimage* 2007; 35: 1409–1423.
22. Watson BD, Dietrich WD, Busto R, et al. Induction of reproducible brain infarction by photochemically initiated thrombosis. *Ann Neurol* 1985; 17: 497–504.
23. Bar-Klein G, Cacheaux LP, Kamintsky L, et al. Losartan prevents acquired epilepsy via TGF-beta signaling suppression. *Ann Neurol* 2014; 75: 864–75.
24. Karhunen H, Bezvenyuk Z, Nissinen J, et al. Epileptogenesis after cortical photothrombotic brain lesion in rats. *Neuroscience* 2007; 148: 314–324.
25. Bragin A, Jando G, Nadasdy Z, et al. Gamma (40-100 Hz) oscillation in the hippocampus of the behaving rat. *J Neurosci* 1995; 15(1 Pt 1): 47–60.
26. Behrens CJ, van den Boom LP, de Hoz L, et al. Induction of sharp wave-ripple complexes in vitro and reorganization of hippocampal networks. *Nat Neurosci* 2005; 8: 1560–1567.
27. Taube JS and Schwartzkroin PA. Mechanisms of long-term potentiation: EPSP/spike dissociation, intradendritic recordings, and glutamate sensitivity. *J Neurosci* 1988; 8: 1632–1644.
28. David Y, Cacheaux LP, Ivens S, et al. Astrocytic dysfunction in epileptogenesis: consequence of altered potassium and glutamate homeostasis? *J Neurosci* 2009; 29: 10588–10599.
29. Zhao S and Fernald RD. Comprehensive algorithm for quantitative real-time polymerase chain reaction. *J Comput Biol* 2005; 12: 1047–1064.
30. Guild SJ, McBryde FD and Malpas SC. Recording of intracranial pressure in conscious rats via telemetry. *J Appl Physiol* 2015; 119: 576–581.
31. Murtha LA, McLeod DD, Pepperall D, et al. Intracranial pressure elevation after ischemic stroke in rats: cerebral edema is not the only cause, and short-duration mild hypothermia is a highly effective preventive therapy. *J Cereb Blood Flow Metab* 2015; 35(4): 592–600.
32. Engel D, Schmitz D, Gloveli T, et al. Laminar difference in GABA uptake and GAT-1 expression in rat CA1. *J Physiol* 1998; 512(Pt 3): 643–649.
33. Hagemann G, Redecker C, Neumann-Haefelin T, et al. Increased long-term potentiation in the surround of experimentally induced focal cortical infarction. *Ann Neurol* 1998; 44: 255–258.
34. Mittmann T and Eysel UT. Increased synaptic plasticity in the surround of visual cortex lesions in rats. *Neuroreport* 2001; 12: 3341–3347.
35. Ferando I and Mody I. In vitro gamma oscillations following partial and complete ablation of delta subunit-containing GABAA receptors from parvalbumin interneurons. *Neuropharmacology* 2015; 88: 91–98.
36. Schoknecht K, Prager O, Vazana U, et al. Monitoring stroke progression: in vivo imaging of cortical perfusion, blood-brain barrier permeability and cellular damage in the rat photothrombosis model. *J Cereb Blood Flow Metab* 2014; 34: 1791–1801.
37. Zweckberger K, Juettler E, Bosel J, et al. Surgical aspects of decompression craniectomy in malignant stroke: review. *Cerebrovasc Dis* 2014; 38: 313–323.
38. Dirnagl U, Iadecola C and Moskowitz MA. Pathobiology of ischaemic stroke: an integrated view. *Trends Neurosci* 1999; 22: 391–397.
39. Gursoy-Ozdemir Y, Qiu J, Matsuoka N, et al. Cortical spreading depression activates and upregulates MMP-9. *J Clin Invest* 2004; 113: 1447–1455.
40. Kuroiwa T, Cahn R, Juhler M, et al. Role of extracellular proteins in the dynamics of vasogenic brain edema. *Acta Neuropathol* 1985; 66: 3–11.
41. Rosenberg GA and Yang Y. Vasogenic edema due to tight junction disruption by matrix metalloproteinases in cerebral ischemia. *Neurosurg Focus* 2007; 22: E4.
42. Risher WC, Ard D, Yuan J, et al. Recurrent spontaneous spreading depolarizations facilitate acute dendritic injury in the ischemic penumbra. *J Neurosci* 2010; 30: 9859–9868.
43. Winkler MK, Chassidim Y, Lublinsky S, et al. Impaired neurovascular coupling to ictal epileptic activity and spreading depolarization in a patient with subarachnoid hemorrhage: possible link to blood-brain barrier dysfunction. *Epilepsia* 2012; 53(Suppl 6): 22–30.
44. Seiffert E, Dreier JP, Ivens S, et al. Lasting blood-brain barrier disruption induces epileptic focus in the rat somatosensory cortex. *J Neurosci* 2004; 24: 7829–7836.
45. Hartings JA, Williams AJ and Tortella FC. Occurrence of nonconvulsive seizures, periodic epileptiform discharges, and intermittent rhythmic delta activity in rat focal ischemia. *Exp Neurol* 2003; 179: 139–149.
46. Neufeld MY, Vishnevskaya S, Treves TA, et al. Periodic lateralized epileptiform discharges (PLEDs) following stroke are associated with metabolic abnormalities. *Electroencephalogr Clin Neurophysiol* 1997; 102: 295–298.
47. Kann O, Papageorgiou IE and Draguhn A. Highly energized inhibitory interneurons are a central element for information processing in cortical networks. *J Cereb Blood Flow Metab* 2014; 34: 1270–1282.
48. Zemankovics R, Veres JM, Oren I, et al. Feedforward inhibition underlies the propagation of cholinergically

induced gamma oscillations from hippocampal CA3 to CA1. *J Neurosci* 2013; 33: 12337–12351.
49. Penttonen M, Nurminen N, Miettinen R, et al. Ultra-slow oscillation (0.025 Hz) triggers hippocampal after-discharges in Wistar rats. *Neuroscience* 1999; 94: 735–743.
50. Dreier JP, Major S, Pannek HW, et al. Spreading convulsions, spreading depolarization and epileptogenesis in human cerebral cortex. *Brain* 2012; 135(Pt 1): 259–275.
51. Pomper JK, Haack S, Petzold GC, et al. Repetitive spreading depression-like events result in cell damage in juvenile hippocampal slice cultures maintained in normoxia. *J Neurophysiol* 2006; 95: 355–368.
52. Maslarova A, Alam M, Reiffurth C, et al. Chronically epileptic human and rat neocortex display a similar resistance against spreading depolarization in vitro. *Stroke* 2011; 42: 2917–2922.
53. Tomkins O, Friedman O, Ivens S, et al. Blood-brain barrier disruption results in delayed functional and structural alterations in the rat neocortex. *Neurobiol Dis* 2007; 25: 367–377.
54. Dugladze T, Schmitz D, Whittington MA, et al. Segregation of axonal and somatic activity during fast network oscillations. *Science* 2012; 336: 1458–1461.
55. Weissberg I, Wood L, Kamintsky L, et al. Albumin induces excitatory synaptogenesis through astrocytic TGF-beta/ALK5 signaling in a model of acquired epilepsy following blood-brain barrier dysfunction. *Neurobiol Dis* 2015; 78: 115–125.
56. Ivens S, Kaufer D, Flores LP, et al. TGF-beta receptor-mediated albumin uptake into astrocytes is involved in neocortical epileptogenesis. *Brain* 2007; 130(Pt 2): 535–547.
57. Lujan R and Aguado C. Localization and targeting of GIRK channels in mammalian central neurons. *Int Rev Neurobiol* 2015; 123: 161–200.